Nuclear Instruments and Methods in Physics Research A 819 (2016) 73–83

Contents lists available at ScienceDirect

Nuclear Instruments and Methods in Physics Research A

journal homepage: www.elsevier.com/locate/nima

Measured and simulated heavy-ion beam loss patterns at the CERN Large Hadron Collider

P.D. Hermes [a,b,*], R. Bruce [a], J.M. Jowett [a], S. Redaelli [a], B. Salvachua Ferrando [a], G. Valentino [a], D. Wollmann [a]

[a] CERN, Geneva, Switzerland
[b] Institut für Kernphysik, University of Münster, Münster, Germany

ARTICLE INFO

Article history:
Received 18 December 2015
Received in revised form
11 February 2016
Accepted 15 February 2016
Available online 23 February 2016

Keywords:
LHC
Collimation
Heavy-ion beams

ABSTRACT

The Large Hadron Collider (LHC) at CERN pushes forward to new regimes in terms of beam energy and intensity. In view of the combination of very energetic and intense beams together with sensitive machine components, in particular the superconducting magnets, the LHC is equipped with a collimation system to provide protection and intercept uncontrolled beam losses. Beam losses could cause a superconducting magnet to quench, or in the worst case, damage the hardware. The collimation system, which is optimized to provide a good protection with proton beams, has shown a cleaning efficiency with heavy-ion beams which is worse by up to two orders of magnitude. The reason for this reduced cleaning efficiency is the fragmentation of heavy-ion beams into isotopes with a different mass to charge ratios because of the interaction with the collimator material. In order to ensure sufficient collimation performance in future ion runs, a detailed theoretical understanding of ion collimation is needed. The simulation of heavy-ion collimation must include processes in which $^{208}Pb^{82+}$ ions fragment into dozens of new isotopes. The ions and their fragments must be tracked inside the magnetic lattice of the LHC to determine their loss positions. This paper gives an overview of physical processes important for the description of heavy-ion loss patterns. Loss maps simulated by means of the two tools ICOSIM [1,2] and the newly developed STIER (SixTrack with Ion-Equivalent Rigidities) are compared with experimental data measured during LHC operation. The comparison shows that the tool STIER is in better agreement.

1. Introduction

The CERN Large Hadron Collider (LHC) [3] is the largest particle accelerator ever built, providing unprecedented energies of up to 7 *Z* TeV.[1] Besides operation with proton beams, it is capable of accelerating and storing heavy-ion beams, making it the second heavy-ion collider ever built and operated [4]. With the ambitious heavy-ion program, the LHC gives valuable contributions to the understanding of the development of the early universe. Already in the past operational periods with $^{208}Pb^{82+}$ beams, collisions at formerly unprecedented energies up to $\sqrt{s} = 8\,Z$ TeV could be produced. For the next running period even higher beam momenta and intensities are envisaged. The LHC is designed for particle momenta of 7 *Z* TeV/*c* with stored beam energies of up to 362 MJ [3], for the case of proton beams. To bend and focus such rigid beams, the LHC is equipped with over one thousand superconducting magnets, most of which are operated at temperatures as low as 1.9 K, which can quench if tiny fractions of the stored beam energy are deposited inside their coils [5]. Beam losses are, however, unavoidable. In order to provide smooth operation, uninterrupted by quenches, the particle losses should be intercepted by a set of movable solid collimators, the LHC collimation system [6,7]. This multi-stage collimation system was designed to intercept protons at large amplitudes with primary collimators that scatter them into secondary and tertiary collimators where they should be absorbed. So far, the system has proven to be very efficient in proton operation and provided good protection of the superconducting magnets, ensuring a successful LHC Run I (2010–2013) without any quench induced by circulating beam losses with stored energies up to 150 MJ. [8].

In heavy-ion operation the stored beam energies are about a factor 100 smaller than for protons, but the collimation efficiency suffers from the fact that heavy ions have a large cross-section for fragmentation processes, which create isotopes of different magnetic rigidities. These fragmented ions leave the cleaning insertion and have often not received an angular kick large enough to hit the secondary collimators. They start deviating from the main beam in

* Corresponding author at: CERN, Geneva, Switzerland.
E-mail address: phermes@cern.ch (P.D. Hermes).

[1] *Z* indicates the charge multiplicity of the hadron, e.g. $Z=1$ for protons and $Z=82$ for $^{208}Pb^{82+}$ ions.

http://dx.doi.org/10.1016/j.nima.2016.02.050

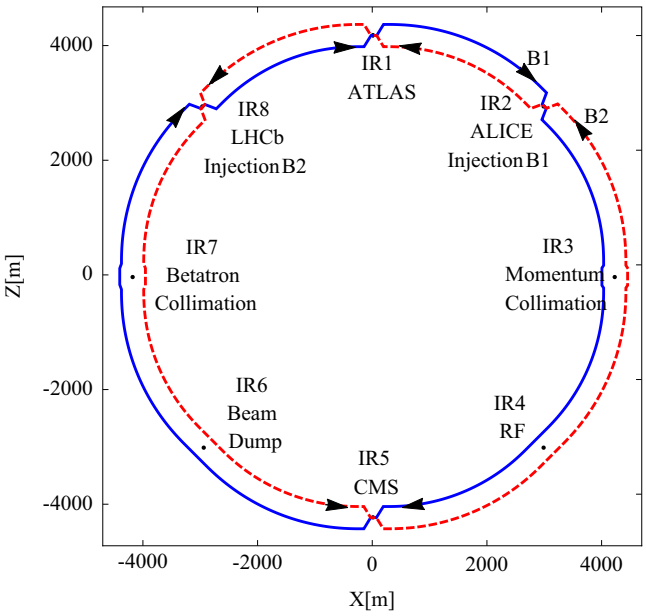

Fig. 1. Layout of the LHC. The machine provides eight straight insertion regions for experiments and other functionalities.

the bending magnets downstream of the collimation insertions where the dispersion rises and thus risk to be lost.

Even if the heavy-ion operation during the LHC Run I up to $4\,Z$ TeV was successful, with the envisaged increase of beam energy and intensity upgrade, the cleaning inefficiency could become critical and limit the achievable intensity and hence also the luminosity. Sophisticated simulation tools are therefore required to predict the ion loss distribution. Based on these simulations, the collimation system can be re-optimized to provide better protection and better upgrade strategies can be defined. In this paper we study the heavy-ion loss patterns in the previous LHC run in both measurements and simulations and compare two different simulation methods.

In Section 2 the LHC and its collimation system are presented. The third section describes the transverse motion of heavy-ion beams and the physical peculiarities of heavy-ion interaction with matter. Measured beam loss patterns during LHC operation are presented in the fourth section. The simulation tools used for heavy-ion collimation simulation are discussed in Section 5. The results of the simulations are discussed and compared to measured heavy-ion beam loss patterns in Section 6 The paper closes with a summary and outlook.

2. The LHC and its collimation system

The LHC is a collider of 27 km circumference installed at the end of a complex accelerator chain at CERN, close to Geneva, Switzerland. It provides high intensity proton or heavy-ion beams that are brought into collision inside the detectors of the main experiments ATLAS [13], ALICE [14], CMS [15] and LHCb [16], installed in four of its eight straight sections, the so-called insertion regions (IR). The four remaining IRs house accelerating RF cavities in IR4, beam dumping system in IR6, betatron collimation in IR7 and momentum collimation in IR3. The individual straight sections are separated by eight arc regions, in which superconducting bending magnets and quadrupoles provide beam transportation to the next IR and adequate focusing. The layout of the machine is schematically illustrated in Fig. 1.

In Table 1 the LHC design parameters for proton and $^{208}Pb^{82+}$ ion beams are shown in comparison to the heavy-ion beam parameters achieved during the operational blocks in 2010, 2011 and 2013.

The cleaning system in IR7 holds multiple collimation stages in which a primary collimator (TCP) intercepts the trajectories of protons at large betatron-amplitudes in order to scatter them to even larger amplitudes into the slightly retracted secondary collimators (TCSG) and the active absorbers (TCLA). Tertiary collimators (TCT) in each IR protect the triplet of quadrupoles around each experiment from the secondary beam halo and abnormal beam losses during failures [17]. They should also minimize experimental background [18]. Depending on their function, the different collimator types are made of different materials such as carbon fibre composite for the TCPs and TCSGs or a tungsten alloy for the TCLAs and the TCTs.

The collimators are mostly assembled with two movable collimator jaws which are adjusted symmetrically around the beam center. The collimator openings are usually given in terms of the local RMS beam size σ, using the nominal emittance and betatron function. They are summarized for previous LHC runs together with the design values in Table 2. Compared to the design settings, larger margins between the collimation stages were chosen at the beginning of LHC operation to avoid hierarchy violations due to machine imperfections [19]. With improving operational experience, the settings have been continuously tightened to provide better protection and thus allow for higher luminosities [17,20]. The nominal retractions have not yet shown a good enough long-term stability of the hierarchy against optics and orbit drifts to be used in standard operation.

To be intercepted by the secondary collimators, the scattering angle in the primary collimator must be at least [2]

$$\Delta\theta_{\min} = \sqrt{\frac{(N_S^2 - N_P^2)\epsilon_N}{\gamma\beta_{\mathrm{TCP}}}}$$

assuming that the secondary collimator is placed at such a phase advance from the TCP that the betatron amplitude is maximized at the prior. Here, N_P and N_S are the half gaps of the primary and secondary collimator normalized by the RMS beam size, ϵ_N is the normalized beam emittance, γ is the relativistic Lorentz factor and β_{TCP} the betatron function at the location of the primary collimator.

The multi-stage approach, with collimator settings optimized for protons, is not efficient for heavy-ions. Scattering to large transverse angles in the collimator material is a small effect compared to the breakup into lighter fragments. Such processes and the motion of ion fragments in the machine are discussed in detail in the next section.

The performance of the collimation system is usually measured in terms of the local cleaning inefficiency describing the number of particles N_{loc} impacting the magnet aperture in an appropriate section of the ring $[s, s+\Delta s]$ normalized by its length Δs and the maximum number of particles impacting at a single location (usually the TCP):

$$\eta(s) = \frac{N_{\mathrm{loc}}(s)}{N_{\max}\,\Delta s}. \tag{1}$$

The graphical representation of the local cleaning inefficiency $\eta(s)$ as a function of the longitudinal position is referred to as a loss map.

3. Ion kinematics

To understand ion loss patterns, it is crucial to quantify the probability for fragmentation processes in the collimator materials. Ion

Table 1
Comparison of the LHC design beam parameters for heavy-ion beams and proton beams in comparison to the parameters achieved in the LHC heavy-ion runs. [3,9–12]. The parameters given for p-Pb operation refer to the $^{208}Pb^{82+}$ beam.

Species	p–p Nominal	Pb–Pb Nominal	Pb–Pb 2010	Pb–Pb 2011	p–Pb 2013
Energy (TeV)	7	7Z	3.5Z	3.5Z	4.0Z
Number of bunches	2808	592	137	358	338
Particles per bunch (10^8)	1.15×10^3	0.7	1.12	1.20 ± 0.25	1.40 ± 0.27
Norm. tr. emittance (μm rad)	3.75	1.5	2.0	1.7 ± 0.2	–
Stored beam energy (MJ)	362	3.81	0.71	1.98	2.18
Peak luminosity (10^{27} cm^{-2} s^{-1})	1.0×10^7	1 (Pb–Pb)	0.03	0.5	110

Table 2
Collimator half gaps, as used in the LHC heavy-ion runs 2011 and 2013 [8] compared to the nominal settings from [3]. The collimator settings are calculated using the design normalized emittance of 3.5 μm rad for protons and the nominal β-functions. The normalized heavy-ion beam emittance is 1.4 μm rad, thus the geometric emittance is identical for protons and heavy-ions since it scales with the relativistic $\sqrt{\gamma^2-1} \approx \gamma$.

Parameter	IR	Unit	2010	2011	2013	Nom.
Energy	–	Z TeV	3.5	3.5	4.0	7.0
TCP	IR7	σ	5.7	5.7	4.3	6.0
TCSG	IR7	σ	8.5	8.5	6.3	7.0
TCLA	IR7	σ	17.7	17.7	8.3	10.0
TCP	IR3	σ	12.0	12.0	12.0	15.0
TCSG	IR3	σ	15.6	15.6	15.6	18.0
TCLA	IR3	σ	17.6	17.6	17.6	20.0
TCT	IR1,IR5	σ	15.0	11.8	9.0	8.3

Table 3
Characteristics of the particle–matter interaction for heavy-ion beams in comparison to proton beams at the LHC design energy [2].

Parameter	Unit	$^{208}Pb^{82+}$	p
Energy	TeV	574	7
$\frac{1}{E}\frac{dE}{ds}$ from ionization	m^{-1}	-7.3×10^{-3}	-8.8×10^{-6}
Mult. scattering ang. (rms)	$\frac{\mu rad}{\sqrt{m}}$	4.72	4.72
Nucl. interaction length	cm	2.5	38.1
EMD length	cm	19	–

fragmentation processes are either caused by electromagnetic dissociation (EMD) or nuclear inelastic fragmentation (NF) [21]. EMD processes occur at photon-induced ultraperipherical encounters of two nuclei and lead to the emission of one or a few nucleons. The cross-section for this process is approximately logarithmically dependent on the energy in the center of mass frame. NF processes are likely to happen from nucleus-nucleus interactions with small impact parameters and have a weak dependence on the energy. They lead to the creation of a broad range of fragments. These fragments can be subject to further fragmentation processes, thus a large variety of different ion types can be produced by the interaction with the collimator material. The relative multiplicities of different ion species depend on the material and the distance traversed. Besides the change of particle species, the fragments may change energy and direction compared to that of the source beam. Further interactions which can cause such energetic or angular kicks are multiple Coulomb scattering (MCS) and energy loss through ionization as described by the Bethe–Bloch formula [22]. Contrary to protons, nuclear elastic scattering is negligible for heavy-ions. Important parameters describing the impact of the different processes for protons and $^{208}Pb^{82+}$ ions are compared in Table 3.

The mass to charge ratio of a generated ion fragment is usually different from the one of the reference ion beam that the magnetic lattice is matched for. The momentum of an ion may be expressed as $P = m\gamma\beta c$, where m is the ion rest mass, β is the particle speed normalized by the speed of light c and γ is the relativistic Lorentz factor. The momentum P per charge q of an arbitrary ion relates as follows to the momentum P_0 per charge q_0 of the reference isotope:

$$\frac{P}{q}\frac{q_0}{P_0} = \frac{\rho}{\rho_0} = \frac{(1+\delta_v)}{\chi} = (1+\delta_{\text{eff}}), \tag{2}$$

where ρ, ρ_0 are the respective bending radii of the tracked ion and the reference isotope, δ_v is the relativistic $\beta\gamma$ of the particle relative to $\beta_0\gamma_0$ of the reference isotope and χ is the mass to charge ratio of the ion relative to the reference isotope:

$$1+\delta_v = \frac{\beta\gamma}{\beta_0\gamma_0} \quad \chi = \frac{q}{q_0}\frac{m_0}{m}. \tag{3}$$

The quantity δ_{eff} describes the rigidity of an arbitrary ion in terms of an equivalent momentum offset of the reference isotope. The motion of an arbitrary ion with a certain set of (χ, δ_v) in the magnetic lattice is identical to the motion of an ion of the reference species with the momentum offset δ_{eff}. If the reference isotope is a proton, the proton momentum P_E with ion-equivalent rigidity is simply given by the ion momentum per charge unit

$$P_E = P_0(1+\delta_{\text{eff}}) = \frac{P}{Z}. \tag{4}$$

In the LHC, the heavy ions are fully stripped nuclei without electrons, thus $Z = q/e$.

4. Heavy-ion losses measured in LHC operation

During operation, a set of approximately 3600 beam loss monitors (BLM) keeps track of the losses throughout the LHC ring. The beam interlock system triggers a beam dump if a certain loss threshold is exceeded [23]. The beam loss monitors are ionization chambers installed at the outer side of superconducting magnets, collimators and other elements, measuring secondary particle showers coming from impacting ions [23,24].

Before operation with high intensity beams, dedicated qualification loss maps are measured with low-intensity beams to verify the collimation efficiency with given optics and collimator settings. High losses at the betatron collimators are induced by crossing the third order tune resonance or by inducing white noise excitation by means of the transverse damper (ADT) [25]. The latter provides better control of the losses and was used in the LHC from 2012 on [25–27]. With the ADT, single bunches can be individually excited in either of the two transverse planes. Momentum cleaning with the IR3 collimation system is probed by means of a momentum shift generated through a change of the RF frequency [8].

In qualification betatron loss maps, each transverse plane is probed individually for each beam. The dominant loss locations are the primary collimators in IR7, where the loss rate should be large enough to provide a sufficiently high signal-to-noise ratio. In this setting, the loss map is dominated by collimation losses, so the loss pattern obtained gives a direct estimate of the cleaning efficiency.

Fig. 2 shows a Beam 1 loss map measured in 2011, compared for the heavy-ion and the proton case at 3.5 Z TeV with identical optical and collimator settings, except in IR2, where the heavy-ion beams were squeezed to $\beta^* = 0.8$ m instead of $\beta^* = 10$ m with protons.[2] The collimator settings are summarized in Table 2. All BLM signals are cleaned from background and normalized to the highest signal, typically seen at the TCP or just downstream. The heavy-ion loss distribution is dominated by losses in the betatron collimators of IR7, followed by the momentum collimators in IR3. Downstream of the betatron collimation region, two loss clusters in the dispersion suppressor region were measured at amplitudes of $\eta_{max} = 10^{-2}$ (two orders of magnitude larger than the DS loss clusters for protons). Four loss peaks at $\eta_{max} = 10^{-4}$ to 10^{-2} are present downstream of the dispersion suppressor in the arc magnets between IR7 and IR8. The losses at the TCT in IR8 are smaller with heavy-ion beams than for proton beams. Two loss peaks in the arc region between IR8 and IR1 are visible in both loss maps, but are larger by 2–3 orders of magnitude for the heavy-ion beam. The TCT losses with ion beam in IR1 are followed by a large loss peak in the arc region between IR1 and IR2, with $\eta_{max} = 10^{-3}$. While IR2 is free of losses beyond the noise level in the proton loss map, four major loss peaks, one being at the TCT, are visible in octant 2 with the heavy-ion beams. The different loss patterns in this region can be explained by the different optical configuration used in the two measurements. The loss rate in IR3 is larger by 2 orders of magnitude for the heavy-ion case, indicating the large number of off-momentum ions which are present in the machine. The losses at the IR5 TCT and the dump protection devices in IR6 are higher with proton beams than with heavy-ion beams.

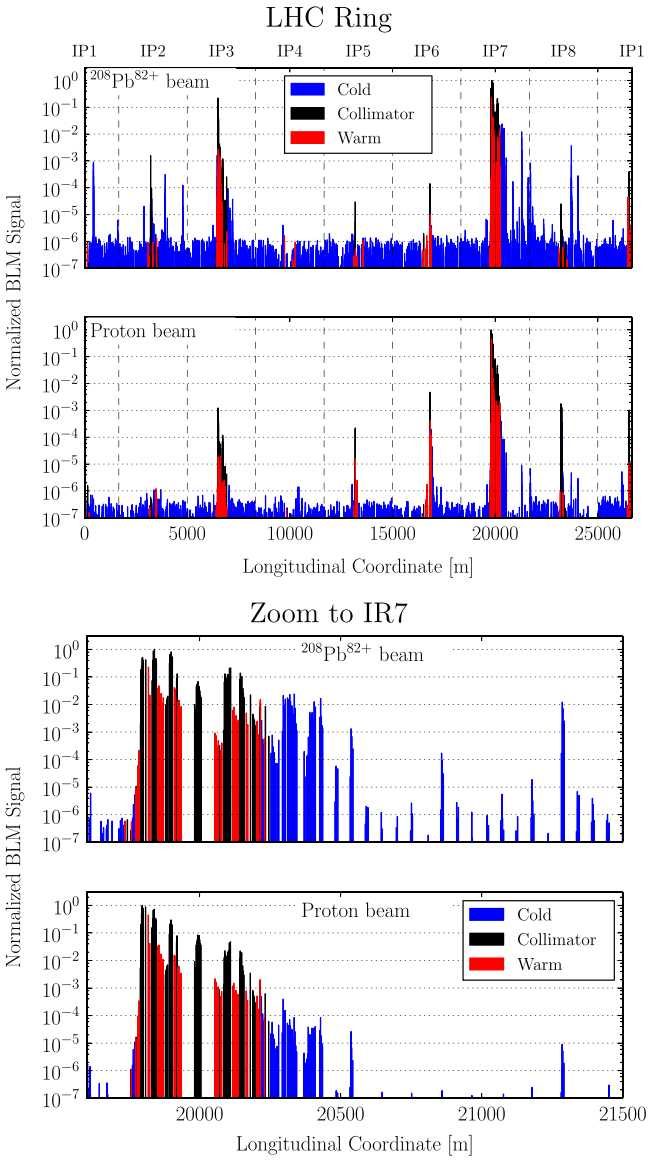

Fig. 2. Qualification loss maps with proton and $^{208}Pb^{82+}$ beams at 3.5 Z TeV with identical collimator settings and optics, except in IR2. The proton loss map is taken from [8]. Both measurements were taken during the 2011 proton and heavy-ion operation. The vertical dashed lines mark the LHC octants. The upper plots show the full LHC ring, the bottom plots a zoom to IR7.

5. Simulation of heavy-ion collimation

The simulation of LHC collimation loss maps for a given optical configuration and with specific collimator settings requires two complementary types of simulation. First, the tracking through the magnetic accelerator lattice, considering the mass and charge of the reference ion and of the tracked ion, which can be done in a simplified manner using P_{eff}. Dispersive effects must be appropriately modelled, particularly if $|\delta_{eff}|$ of the tracked ion is large. Secondly, a Monte-Carlo simulation of the particle interaction with matter is required to account for the scattering and fragmentation of the ions. This requires the knowledge of the momentum, angle of incidence and species of the tracked ion, as well as the material properties and geometry of the collimator jaw at which the interaction takes place. The resulting ion distribution is then further tracked to simulate where a large number of particles intercept the magnet aperture.

We use two different tools to simulate the heavy-ion collimation efficiency, called ICOSIM (Ion Collimation Simulation) [1,2] and STIER (SixTrack with Ion-Equivalent Rigidities). In the generated loss patterns, the contribution of each ion is weighted by the number of nucleons, which represents approximately the scaling of the deposited energy for different ion species.

[2] The β^*-value corresponds to the β-function at the interaction point.

5.1. Ion collimation simulation (ICOSIM)

ICOSIM [1,2] was the first tool developed for the simulation of heavy-ion collimation at the LHC and gave the estimates on heavy-ion loss patterns before the first LHC heavy-ion run in 2010. ICOSIM has also been successfully used to simulate heavy-ion loss patterns in the CERN Super Proton Synchrotron (SPS) [28]. The software provides an integrated environment with a heavy-ion tracking routine for the magnetic lattice and a Monte-Carlo module to simulate the interaction of different heavy-ions with matter.

An initial tracking is realized by means of a linear mapping using transfer matrices between primary collimators for 10^5 turns to get the impact coordinates on the collimators. Every 100 turns, the beam is artificially blown up using random kicks in order to simulate diffusion. The diffusion speed is chosen by the user and changes the depth of impact at the primary collimators. Alternatively, the simulation can be

initiated with the particles starting as an annular halo in transverse phase space with amplitudes large enough to intercept the primary collimators already at the first turn. In this case, the outer edge of the phase space ellipse enclosing a volume of $\epsilon \approx \sigma_{\mathrm{TCP}}^2/\beta$, with σ_{TCP} as the half gap of the primary collimator, is evenly populated [8]. Such an annular halo is used in SixTrack for proton studies.

After the initial phase of linear tracking, particles are tracked element-by-element including chromatic effects in leading order and sextupoles in thin-lens approximation, starting from the turn when they hit the primary collimator in the linear tracking. During this second phase, the Monte-Carlo code for the fragmentation and scattering in collimators is activated.

The software tracks the array $(x, x', y, y', \delta_v, A, Z)$ to describe the transverse beam dynamics and track the ion species. The code can thus handle multi-isotopic particle beams with different values of χ. At every element, the particle positions are compared with the available aperture and particles are removed from the tracking, once the aperture is intercepted. RF elements are not included in the simulation, since the synchrotron oscillation period is assumed to be large compared to the typical distances the fragments travel inside the machine.

The Monte-Carlo code is capable of computing energy loss through ionization using the Bethe–Bloch equation [22]. Multiple Coulomb scattering (MCS) is simulated in Gaussian approximation, as described by the Molière formula [22]. Nuclear fragmentation and electromagnetic dissociation processes are simulated in a simplified manner, using tabulated cross-section tables which we compute beforehand using a Monte-Carlo event generator such as FLUKA (FLUktuierende KAskade) [29,30]. FLUKA contains regularly improved physics models, and tracks the particles of the initial beam together with secondary particles generated from electromagnetic or hadronic cascades. The geometry of the studied material and the beam properties are given by the user via a dedicated input file. The obtained cross-section tables carry information about the probability of a fragmentation process into specific ions.

After the computation of the interaction, ICOSIM either gives the particle back to the tracking routine, with updated information on the ion species, or removes the particle from the tracking if it was absorbed inside the collimator. In the ensuing magnetic tracking of ions that exit a collimator and continue along the lattice, only the heaviest fragment in each interaction is considered, assuming that the light fragments are lost closely to the collimator where the fragmentation occurred. Furthermore, kicks in angle and energy from the fragmentation process are neglected, thus $\Delta p = \Delta\theta = 0$. Cross-section tables are computed for many isotopes, enabling further fragmentation simulations of ion fragments at sub-sequent collimators. Optics and collimator settings are read from dedicated input files. The optics can be imported from MAD-X [31].

For the presented simulations an initial particle distribution of 10^6 particles is generated as an annular halo of $^{208}\mathrm{Pb}^{82+}$ ions to have starting conditions identical to SixTrack. The simulation is carried out for 500 turns, enough to make most of the initial $^{208}\mathrm{Pb}^{82+}$ ions interact with a collimator.

5.2. SixTrack with ion-equivalent rigidities (STIER)

SixTrack with ion-equivalent rigidities (STIER) [32] is developed in the assumption that the heavy-ion beam loss pattern is mainly defined by ion fragments from the interaction of the main beam with the primary collimator. It was used to predict the ion cleaning efficiency after potential HL-LHC upgrades [33]. STIER uses as starting conditions the distributions of ion fragments exiting the primary collimator, but using a more detailed model than ICOSIM and neglects fragmentation in sub-sequent collimators. STIER is not an integrated simulation tool, but bases upon a three-step simulation chain consisting of

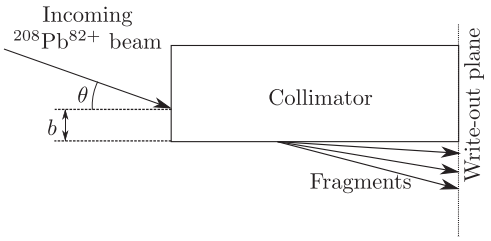

Fig. 3. Schematics of the initial fragmentation simulation for STIER. An heavy-ion beam impacts the collimator material, modelled as a simple block of carbon of 60 cm length, with the impact parameter b at an angle θ.

1. Optics calculation,
2. Ion fragmentation simulation at the TCP,
3. Magnetic tracking through the accelerator lattice.

In a first step, the optical configuration of the machine is computed using MAD-X. With the Twiss parameters obtained, the phase space parameters of particles impacting the primary collimator can be computed.

In a second step, the fragmentation is simulated by means of FLUKA. The fragmentation simulation carried out for the presented study is schematically illustrated in Fig. 3. The initial beam of $^{208}\mathrm{Pb}^{82+}$ ions hits the collimator material, which is modelled as a 60 cm block of carbon, at an angle θ with an impact parameter b. The angle θ is known from the prior optics calculation. The information on out-coming particles is then transformed into starting conditions of protons with equivalent magnetic rigidity for the sub-sequent tracking simulation using Eq. (4). This approach has the intrinsic advantage that all ion fragments can be included in the tracking with their respective momenta and angles including eventual kicks from the fragmentation.

As a third step, the ion fragments are tracked through the magnetic lattice by means of the symplectic particle tracking code SixTrack [34–37]. The software is designed to provide multi-turn proton tracking at relativistic energies and used for all single particle simulations for LHC and HL-LHC. It is the standard tool for the simulation of proton collimation at the LHC. For this purpose it has been shown to be in excellent agreement with measured LHC data [8]. Transformations of the particle coordinates at the individual accelerator lattice elements are computed by the usage of symplectic transfer maps in the thin element approximation. The accelerator lattice with the corresponding optics settings is read from an input file which may be generated by MAD-X. Details of the beam properties and collimator settings are given by a dedicated input file. Particle losses on the aperture are identified with a precision of $\Delta s = 10$ cm by comparing the individual particle tracks to a detailed model of the LHC aperture.

SixTrack provides tracking only for protons, thus $\chi = 1$ for all tracked particles. Therefore, in its native form SixTrack is not a candidate to provide heavy-ion tracking. Accurate ion tracking can, however, be accomplished if proton momenta with ion-equivalent rigidities are used. The built-in Monte-Carlo routine to simulate proton-matter interaction is evaded by setting the collimator materials to perfect absorbers. The particles are assumed to start at the location of the collimator jaws, which are at a large enough transverse amplitude so they can expected to be lost within a few turns. Therefore the tracking is done for 100 turns, enough for almost all ion fragments to be lost on the machine aperture.

Due to the absence of a fragmentation simulation at subsequent collimators, the simulated losses at the collimator locations are over-estimated in this approach. Furthermore, loss peaks

in the aperture from fragmentation at sub-sequent collimators are not included in this simulation.

6. Simulation results

The presented simulation tools are used in different configurations to study the impact of the various simplifications used in the two tools. As study case we use ICOSIM and STIER to simulate $^{208}Pb^{82+}$ losses from the horizontal IR7 TCP collimator in the 2011 machine configuration with $\beta^* = 3$ m at LHCb and $\beta^* = 1$ m at the remaining experiments with a beam energy of 3.5 Z TeV. The applied collimator settings are summarized in Table 2. Based on previous studies with proton beams, an impact parameter of 3 μm is considered realistic [8]. However, this assumes the diffusion mechanisms as for proton beams, which could be different with respect to heavy ions. Therefore we perform the simulation with different impact parameters $b = 1$ μm, $b = 3$ μm and $b = 10$ μm.

The ICOSIM simulation is carried out with the same optics and collimator settings as the STIER simulation. A simplified STIER simulation is realized using all isotopes from the fragmentation simulation but neglecting eventual deviations in angle and energy $\Delta p = \Delta\theta = 0$. With this simulation we study the change of the simulated loss pattern with respect to ICOSIM, if all isotopes were included. In the second, complete, STIER simulation, the loss pattern is studied when the angles and energies of all fragments leaving the collimator are taken into account. Besides the more accurate modelling of the initial fragment conditions, STIER has the advantage that fragments starting from the two collimator jaws can be studied individually, which is done in a third STIER simulation. The STIER simulation results are also compared for the three mentioned impact parameters. Finally, we compare the tracking routines of the two simulation codes for different isotopes to conclude on the improvements with the better chromatic modelling in SixTrack.

6.1. Simulation of initial conditions for STIER

With the simulation parameters discussed above, an initial sample of 10^7 incoming $^{208}Pb^{82+}$ ions is fragmented into 3×10^8 hadronic fragments. The simulated energy fractions carried by the individual isotopes, normalized to the total beam energy of the out-coming ions, are shown in Fig. 4. The obtained coordinates are used to compute initial conditions for the SixTrack simulation. The particles are supposed to start at the horizontal TCP in IR7, vertically centered without an initial angle in the vertical direction. Comparisons to simulations with a Gaussian distribution in y, y' have shown that the loss pattern in unchanged in this approximation.

6.2. Loss map simulations

The result of the ICOSIM simulation is shown in the first row of Fig. 5 for the full LHC ring (left) and zoomed into IR7 and the following arcs (right). Fragments scattered out of the collimators are in this model absorbed closely to the collimators where the fragmentation occurred and do not continue moving inside the machine for long distances. Losses in warm regions are visible only in IR3 but not in IR7. The mass number of the heaviest created and tracked fragment is $A_{max} = 90$ which can be traced back to the simplified fragmentation algorithm. The high measured loss peaks (see bottom row in Fig. 5) in the arcs between IR7 and IR8 are, with one exception, not reproduced by ICOSIM. The most critical losses in the dispersion suppressor located in the cells 8 and 9 of IR7 are visible in the simulated loss map. The local cleaning inefficiency in this region peaks at approximately $\eta = 10^{-2}$, which is comparable to the measured loss distribution. Note that the

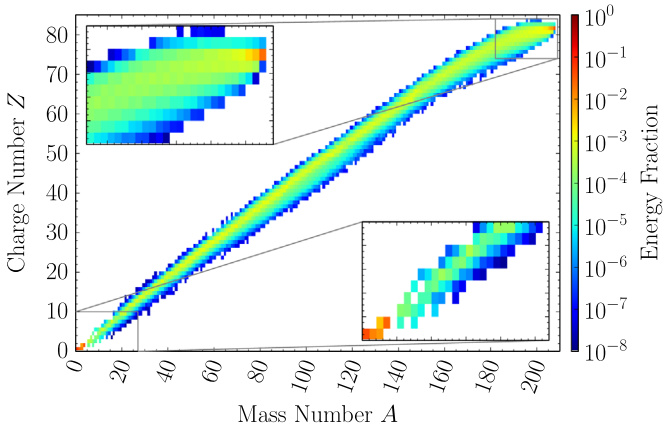

Fig. 4. Energetic fractions of the individual isotopes emerging from the IR7 horizontal TCP from an impacting $^{208}Pb^{82+}$ beam at 3.5 Z TeV, simulated with FLUKA as shown in Fig. 3 with an impact parameter of $b = 3$ μm. The energy fraction is computed by multiplying the isotope abundance $N(A,Z)$ with the nucleon number A and the momentum per nucleon $p(A,Z)$ and normalizing by the total ion energy coming out of the collimator $\sum_{A,Z} A \times N(A,Z) \times p(A,Z)$. It is assumed that the momentum per nucleon is approximately identical for all ions $p(A,Z) \approx p$.

presented loss map simulations provide full azimuthal coverage in the detection efficiency of lost particles. In reality, however, the BLM detectors have limited azimuthal coverage and only measure secondary particle showers of lost ions, which vary depending on the local machine geometry and materials. Therefore, the measured loss signals cannot be directly compared to simulated loss patterns. However, the simulations still give indications about the longitudinal loss patterns and critical loss positions in the machine.

The loss maps from the simplified STIER simulation are shown in the second row of Fig. 5. The losses are more broadly distributed over the LHC ring when the full spectrum of fragments is included. This indicates that light isotopes are by no means only lost locally in the secondary collimators or in the warm regions surrounding them. Parts of the losses in the warm region of IR7 are reproduced in this simulation approach, originating mainly from very light isotopes at $|\delta_{eff}| \gg 0$. The two clusters of losses in the IR7 DS are increased in their intensity and longitudinal extension, since the isotopes which are neglected in ICOSIM are now included and are lost in these regions. The loss peak with the largest amplitude is still in the IR7 DS but is increased to $\eta_{max} = 10^{-1}$. One of the loss peaks in the arcs is, as in ICOSIM, reproduced in this simulation. Also here, the simulated peak intensity is increased with respect to ICOSIM.

The loss maps generated with the full STIER simulation are shown in comparison to the measurement and the ICOSIM loss map in the third row of Fig. 5. This approach shows the best agreement with the measured loss distribution. The four highest loss peaks in the arcs become visible when the angles and energies of the fragments are included.

A larger amount of losses in the warm IR7 magnets (W1) is visible, coming mainly from the very light fragments scattered out of the collimator (see Table 4 for the isotopes that contribute most to these losses). The two loss clusters (C1 and C2) in the IR7 DS are modelled with a correct longitudinal extension and order of magnitude (the mainly contributing isotopes to C1 and C2 are also listed in Table 4). It is remarkable that the second loss cluster C2 is dominated by heavy fragments of Pb, created by electromagnetic dissociation (the three isotopes contribute to 61.8% of the total deposited energy), while the highest fraction of C1 is due to very light isotopes (H and He ions) where the four most important isotopes only compose only 19.5% of the energy deposited in C1. With 1227 different isotope species lost in C1, the deposited

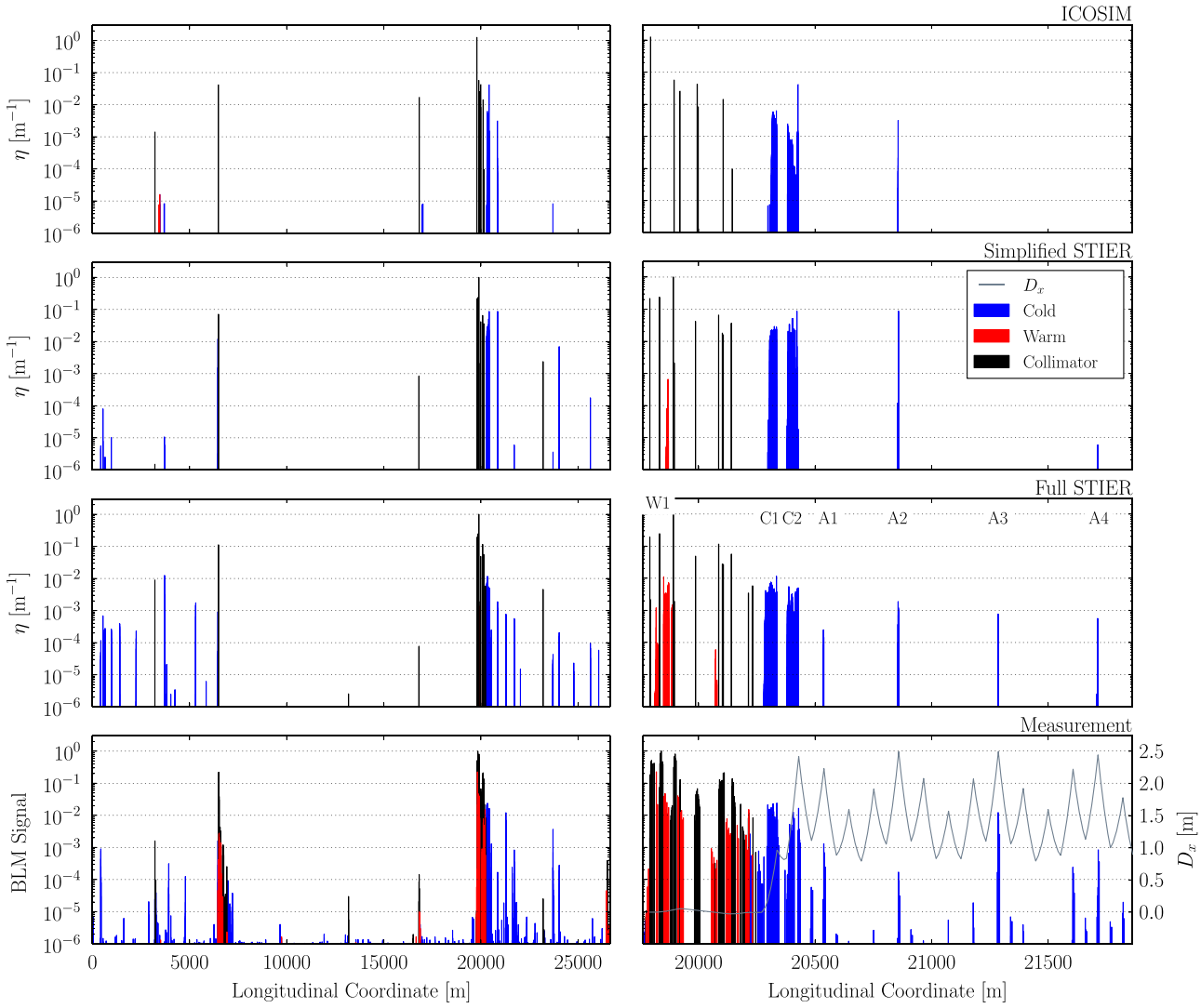

Fig. 5. Comparison of loss map simulations using ICOSIM (top row), a simplified STIER approach (second row), a full STIER simulation (third row) and the measured loss maps during the 2011 LHC heavy-ion run at 3.5 Z TeV. The right graph in the bottom row also shows the locally generated dispersion function D_x starting at $D_x=0$ at the TCP. The left column shows the loss map over the full LHC ring, while the right column shows the same loss map zoomed into the betatron collimation region IR7. The STIER simulations are carried out assuming an impact parameter of $b=3$ μm.

Table 4
STIER simulated contributions on the total deposited energy at the warm magnets in IR7 (W1), the two loss clusters in the IR7 DS (C1 and C2) and in the arcs downstream of IR7 (A1,A2,A3,A4) as shown in Fig. 5.

W1		C1		C2		A1		A2		A3		A4	
Ion	(%)	Ion	(%)	Ion	(%)	Ion	(%)	Ion	(%)	Ion	(%)	Ion	(%)
$^{1}H^{1+}$	57.0	$^{3}H^{1+}$	8.6	$^{206}Pb^{82+}$	34.0	$^{204}Tl^{81+}$	61.0	$^{204}Tl^{81+}$	74.6	$^{204}Tl^{81+}$	86.6	$^{204}Tl^{81+}$	86.7
$^{3}H^{1+}$	38.0	$^{4}He^{2+}$	4.5	$^{205}Pb^{82+}$	16.2	$^{206}Pb^{82+}$	18.7	$^{206}Pb^{82+}$	10.3	$^{199}Au^{79+}$	6.7	$^{199}Au^{79+}$	7.2
$^{2}H^{1+}$	2.6	$^{2}H^{1+}$	3.2	$^{204}Pb^{82+}$	11.6	$^{199}Au^{79+}$	7.4	$^{199}Au^{79+}$	5.7	$^{206}Pb^{82+}$	2.2	$^{206}Pb^{82+}$	1.7
$^{3}He^{2+}$	1.4	$^{203}Pb^{82+}$	3.2	$^{203}Tl^{81+}$	8.7	$^{1}H^{3+}$	3.5	$^{201}Hg^{80+}$	2.3	$^{194}Ir^{77+}$	1.2	$^{202}Hg^{80+}$	1.6

energy is shared between a much larger number of isotopes than at C2, where only 334 different isotopes are absorbed.

The distributions of the quantity χ for the isotopes lost in the regions C1, C2 are graphically represented in Fig. 6. As expected, the aperture in the cold region C1 captures a very broad range of isotopes. In the cold region C2, mostly isotopes with mass to charge ratios close to the reference ion species contribute to the total deposited energy.

The graph at the right bottom of Fig. 5 shows also the locally generated dispersion function D_x starting at the primary collimator. The dispersion increases from $D_x \approx 0$ m in the warm IR7 magnets to $D_x \approx 1$ m at the end of the C1. At the second loss cluster C2, the dispersion increases to even $D_x = 2.4$ m. We conclude that the isotope distribution shown in Fig. 6 can be explained by the fact that the isotopes with large momentum offsets are removed from the beam already in the C1, while the isotopes with rigidities closer to the main beam are not sufficiently off-momentum to be intercepted by the aperture at this location. When the dispersion further increases at C2, also the isotopes with smaller $|\delta_{\text{eff}}|$ are lost in the aperture, while the isotopes with $A < 190$ have already been removed from the beam in

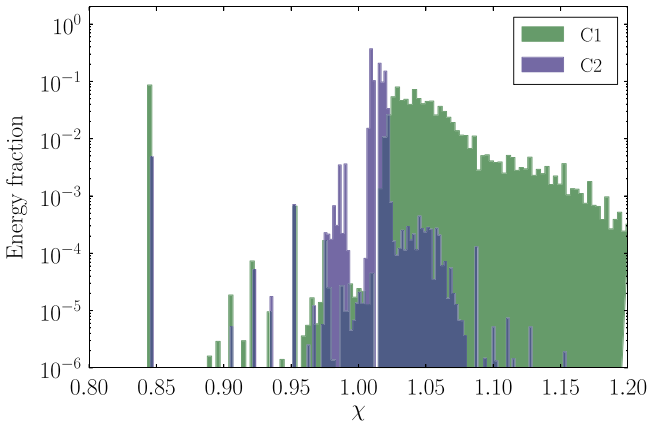

Fig. 6. Fractions of the total deposited energies in the regions C1 and C2 as a function of the relative mass to charge ratio χ. The data is extracted from the full STIER simulation with $b = 3$ μm.

C1. Here it shall be pointed out that the fraction of light isotopes depends strongly on the chosen impact parameter for the fragmentation simulation.

Contrary to this, the isotope composition at the arc loss peaks (A1, A2, A3, A4) is very homogeneous (see Table 4). At the passage through the arcs, the locally generated dispersion function is beating with amplitudes between $0.8\ \text{m} < D_x < 2.5\ \text{m}$. The loss peaks A1–A4 are located at local maxima of the function D_x. The similarity of their isotopic composition can be explained by the fact that, especially for isotopes with rigidities closely to the main beam, the individual starting conditions at the TCP (starting angle and collimator jaw) can partly compensate or enhance dispersive effects, thus some ions of the same species can travel for longer distances than others. It shall be emphasized that except $^{1}H^{3+}$, all isotopes listed for A1–A4 in Table 4 are also included in the ICOSIM simulation. We conclude that the decisive properties determining at which of the four locations a particle is absorbed are the angle and momentum at which the particle is emitted at the TCP, which are not included in ICOSIM. Hence, an accurate simulation of heavy ion loss patterns requires inevitably the incorporation of angular and energetic shifts by fragmentation at the collimator, which should be considered for future simulations.

The fraction of nucleons which is absorbed in the aperture was calculated to be $f_{\text{glob}} = 0.167$, almost two orders of magnitude larger than for comparable simulations with proton beams where this quantity takes typically values in the order of $f_{\text{glob}} = 0.002$ [8].

Parts of the losses far downstream of the TCP are longitudinally shifted with respect to the measured loss peaks in the same region of the LHC. These shifts could come from small aperture displacements in the real machine, or offsets of the closed orbit by the same amount. An analysis of the particle trajectories at the corresponding loss locations shows that displacements as small as $\Delta a = 300$ μm are sufficient to shift the loss location of the impacting ions, while at the loss peaks A1–A4 displacements of $\Delta a > 600$ μm are required for a significant reduction of the loss peak amplitude. Another possible explanation is that a non-equal amount of secondary ion fragments is produced at the two collimator jaws, which is studied in the next sub-chapter.

6.3. Separated STIER simulations for the two TCP jaws

An intrinsic advantage of the STIER setup is the possibility to study the loss behaviour of isotopes starting at the individual collimator jaws. So far, all STIER results assume the same amount of ions impacting on the two TCP jaws. However, studies with proton beams have shown that the beam halo in the real machine can impact the two collimator jaws asymmetrically, as discussed in

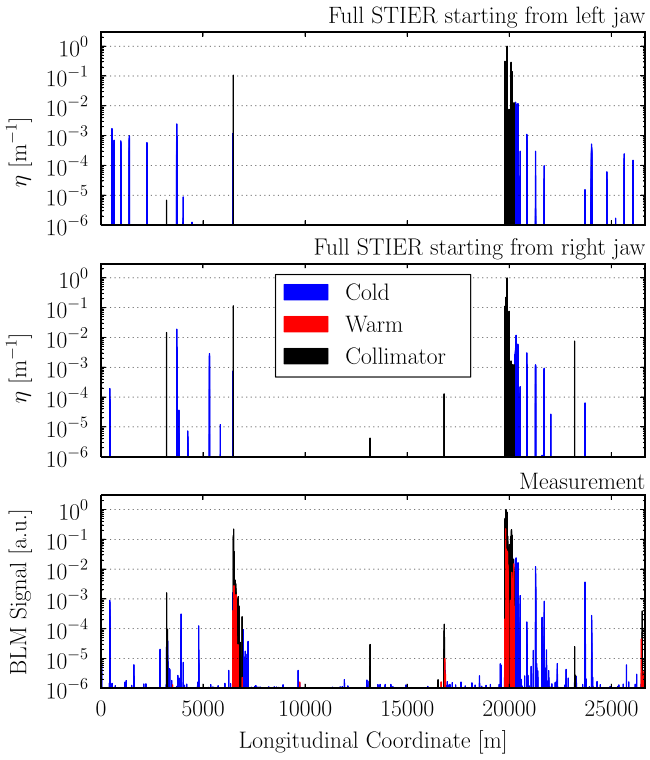

Fig. 7. STIER simulations starting at the left and right collimator jaw, shown in comparison to the measured loss map. The simulations are carried out considering an impact parameter of 3 μm.

[8] and seen from SixTrack simulations. This process is very hard to model accurately in simulations, as it depends on the interplay of a large number of machine imperfections that are not well known. In Fig. 7, the loss map is shown, as simulated with STIER with the same settings as above for particles starting at the left and right collimator jaw separately. A different behaviour of the losses can be expected because the betatronic motion and the dispersion can amplify or compensate each other, depending on the starting conditions of the ion.

From the obtained loss maps it can be seen that the simulation result for the particles starting at the right collimator jaw is in much better agreement with the measured data than for particles starting at the left jaw.[3] The largest fraction of the loss peaks between IR8 and IR1 as well as between IR1 and IR2 which are unobserved in the measurement but visible in STIER come from particles starting at the left jaw. However, one intense peak, visible in the simulation for the right jaw, is unobserved in the measurement, which might come from aperture or orbit displacements as discussed above. In conclusion, the discrepancies of STIER in the regions far downstream of the TCP might come from both asymmetric losses at the two collimator jaws and small beam displacements relative to the aperture.

6.4. STIER with different impact parameters

In the real machine, the impact parameter b of the ions hitting the collimators may vary. For the STIER simulations presented so far, an impact parameter of 3 μm was assumed, based on previous proton studies. As shown in Table 3, the interaction lengths for fragmentation processes by EMD and NF are smaller than the length of the jaw of the primary collimator (60 cm). With

[3] Note that for Beam 1 the left hand side refers to the outer side of the ring and vice versa for Beam 2. We remind that the study is carried out for Beam 1.

Table 5
Isotopes with the largest energetic fractions coming out of the collimator material from the initial fragmentation simulation.

Isotope	Energetic fraction with		
	$b = 1$ μm	$b = 3$ μm	$b = 10$ μm
$^{1}H^{1+}$	4.7×10^{-2}	6.3×10^{-2}	4.0×10^{-1}
$^{2}H^{1+}$	2.1×10^{-2}	2.5×10^{-2}	1.2×10^{-1}
$^{3}H^{1+}$	1.5×10^{-2}	1.7×10^{-2}	7.4×10^{-3}
$^{3}He^{2+}$	5.8×10^{-3}	8.1×10^{-3}	4.9×10^{-3}
$^{4}He^{2+}$	3.6×10^{-2}	4.2×10^{-2}	1.6×10^{-1}
$^{205}Pb^{82+}$	7.1×10^{-3}	2.3×10^{-3}	1.1×10^{-5}
$^{206}Pb^{82+}$	1.7×10^{-2}	5.0×10^{-3}	1.4×10^{-5}
$^{207}Pb^{82+}$	3.3×10^{-2}	8.4×10^{-3}	1.0×10^{-5}
$^{208}Pb^{82+}$	3.6×10^{-2}	8.8×10^{-4}	1.4×10^{-5}

increasing impact parameter, the traversed distance of the heavy-ion beam inside the material increases, leading to a drastic change of the fragmentation rates into the different isotopes. In particular the production of very light ion fragments, such as protons, α-particles and neutrons increases, while the rate of surviving ions of the main beam drops significantly with increasing b. An overview of the energetic fraction carried by different out-coming isotopes after the ion-collimator interaction is given in Table 5. Note that the values are scaled with the ion mass, so the ion abundance is reduced by a factor of A with respect to the given values. With an impact parameter of $b = 3$ μm, the two most important isotopes are protons and α particles followed by $^{208}Pb^{82+}$ ions of the initial species.

The loss maps as simulated with STIER for the three different impact parameters $b = 1$ μm, $b = 3$ μm, $b = 10$ μm are compared in Fig. 8. The loss patterns are qualitatively similar but the loss peak intensities differ quantitatively. For the smallest impact parameter, the highest losses occur at the primary collimator in IR7. The main contribution of these losses comes from $^{208}Pb^{82+}$ ions that were not fragmented but scattered at small angles in the TCP. They move inside the machine for one or multiple turns until they are intercepted by the global bottleneck, which is the primary collimator. In reality, however, these ions are again subject to fragmentation and scattering inside of the TCP, which is not considered in the presented simulation. The losses at the DS region peaks at $\eta = 10^{-3}$, which is smaller than in the other simulations, due to the large amount ions of the main beam surviving the initial passage through the TCP. The remaining losses in the aperture and the other collimators are located at elements which are also subject to losses for the other impact parameters, but the loss amplitudes are smaller. For the cases of $b = 3$ μm and $b = 10$ μm the highest losses are visible at the secondary collimator, which is consistent with the loss pattern measured during operation. Both simulated loss patterns are dominated by ion fragments instead of ions of the main beam. The losses in the DS clusters peak at $\eta = 10^{-2}$ for $b = 3$ μm and are larger by a factor of 3 for the case of $b = 10$ μm. In the latter case, the production yield of effectively off-momentum isotopes is highest among the studied scenarios, which becomes apparent by the comparatively small amount of fragments captured by the collimation system.

A quantitative comparison of the single pass losses at the locations between the TCP and the end of the dispersion suppressor shows that the integrated DS losses normalized by the total losses in this region differ by a factor of 2.3 between the simulation with $b = 1$ μm and $b = 3$ μm. This is likely an artefact caused by the neglection of sub-sequent scattering in the secondary collimators. We can use these discrepancies as an estimate of the uncertainty on the simulation. It should be noted that

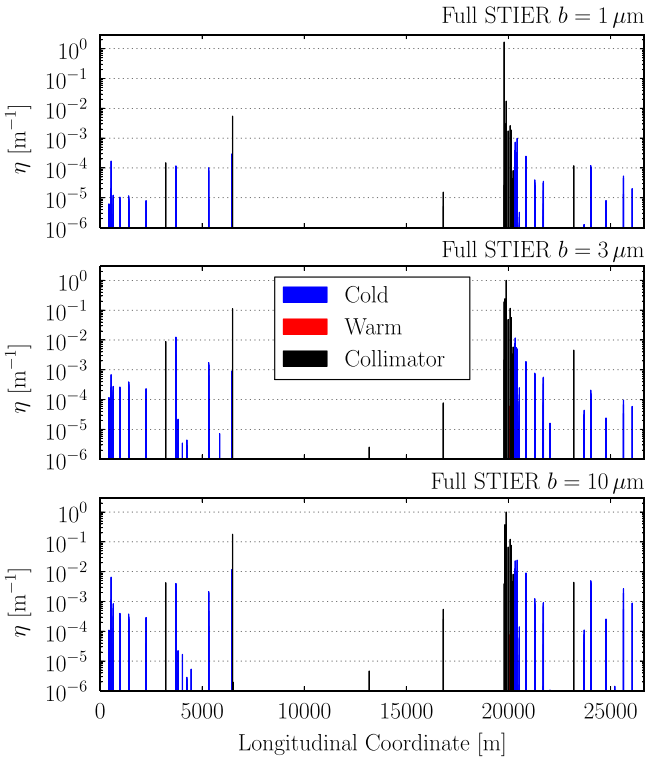

Fig. 8. Ion loss maps as simulated with the full STIER approach for three different impact parameters $b = 1$ μm, $b = 3$ μm, $b = 10$ μm. Losses $\eta < 10^{-4}$ are neglected in order to select loss of the peaks with enough statistics.

discrepancies of similar magnitude have been found in comparisons between simulations and BLM measurements for protons, even after the full shower is included [8]. Between the simulations with $b = 3$ μm and $b = 10$ μm the integrated DS losses are different by only 30% proving that the change of production yields for different isotopes does not lead to a significant change of the loss rates in the cold magnets. The losses in the DS are caused by many different isotopes, such that the rearrangement of the relative isotope abundances does not change the simulation result significantly.

We conclude that the impact parameter does slightly change the local cleaning inefficiency but not the longitudinal loss distribution. The overall dependence of the impact parameter on the simulated loss map can be considered to be small.

6.5. Comparison of the chromatic models of ICOSIM and SixTrack

The chromatic modelling in ICOSIM is done in linear approximation, while SixTrack provides full symplectic 6D tracking. The expected deviations of the computed particle trajectories are small for particles with $|\delta_{\text{eff}}| \approx 0$, but increase for particles with large effective momentum offsets. To study this effect, we perform two tracking simulations with identical starting conditions at the TCP using SixTrack and ICOSIM. The tracks are computed for the two different isotopes, $^{8}Li^{3+}$ and $^{207}Pb^{82+}$, assuming that both start at the TCP with the same angle (the angle of incidence used for the fragmentation simulation) with the momentum per nucleon of the initial $^{208}Pb^{82+}$ beam. The difference in the bending behaviour results from the different mass to charge ratios, quantified as $\chi_{\text{Li}} = 1.054$ and $\chi_{\text{Pb}} = 0.995$. The tracks are illustrated in Fig. 9.

For the $^{207}Pb^{82+}$ ion, with small δ_{eff}, the simulated tracks are different by 200 μm after a distance of 3 km. With the light $^{8}Li^{3+}$ fragment, significant deviations between the simulated tracks

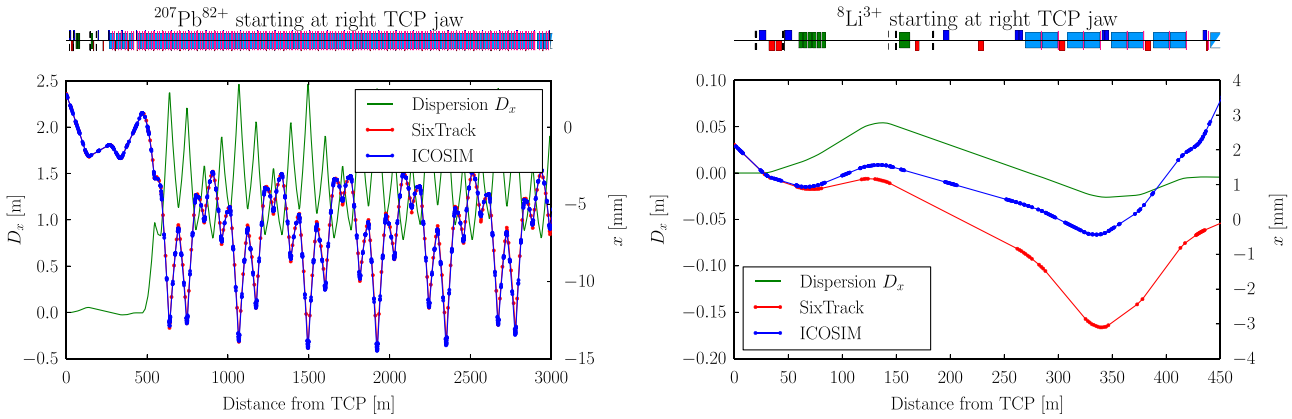

Fig. 9. Comparison of the tracking behaviour of ICOSIM and SixTrack for the two isotopes $^{207}Pb^{82+}$ (left) and $^{8}Li^{3+}$ (right) with identical starting conditions at the right jaw of the IR7 horizontal TCP. Note the different scales for the dispersion function and the computed horizontal position. The elements of the LHC beam line are shown on top of the graphs.

occur after only a few magnets. The particle tracks differ by approximately 3 mm after only 450 m.

Such deviations can significantly change the simulated loss maps. Given that there are numerous ions with even larger effective momentum offsets (e.g. for protons $\chi_p = 0.39$) the tracking of such fragments must be carried out with a more elaborated chromatic tracking algorithm than used in ICOSIM. The light fragments can, as discussed in Section 6.2 contribute significantly to the losses not only locally at the collimators. Based on this result, SixTrack appears to be the better candidate to provide heavy-ion tracking, especially if the light fragments should be included in the simulation.

7. Summary and outlook

The CERN Large Hadron Collider is advancing into unrivalled regimes in terms of stored beam energy and both the LHC proton program and the heavy-ion programs envisage a further increase to provide more luminosity to the experiments. This puts high demands on the collimation system, which so far provided excellent cleaning with proton beams. However, the cleaning efficiency with heavy-ion beams is worse by two orders of magnitude, due to the high production yield of effectively off-momentum ion fragments in the primary collimators, from which many are absorbed in the aperture of superconducting magnets in dispersive regions of the machine. The cleaning performance was sufficient for the previous heavy-ion runs, but it could impose a limitation for the larger intensities foreseen for future operation.

So far, tools available to predict collimation performance and beam losses of heavy-ion beams provided only approximated views of the measured loss maps, without accurately reproducing all loss locations. To better understand and predict the heavy-ion cleaning efficiency, we simulated heavy ion beam losses in the configuration of the LHC $^{208}Pb^{82+}$ ion run in 2011 using two tools, ICOSIM and STIER. The latter is a new tool developed to overcome the simplifications which were assumed to limit the accuracy of ICOSIM. The comparison shows that the STIER approach is in significantly better agreement with the measured data, mainly due to the inclusion of all light ion fragments and the kicks in angle and kinetic energy from the fragmentation inside the collimator.

The STIER simulation was also performed separately for ion fragments starting at the two individual collimator jaws. The simulated case of particles starting from the right collimator jaw shows a better agreement with measurements. It is possible that, in reality, the two collimator jaws are impacted asymmetrically. Furthermore, remaining discrepancies between the measured data and STIER could arise from orbit or aperture offsets in the real machine.

The influence of the impact parameter on the simulated STIER loss pattern was studied and showed some differences in the cleaning inefficiencies which we could trace back to the different production yields of the various isotopes. However, the loss locations did not change.

Finally, the chromatic tracking was studied. It was shown that the discrepancy in the simulated tracks between the linear chromatic modelling of ICOSIM and full 6D symplectic tracking in SixTrack (as part of the STIER approach) is significant for momentum offsets of about 1%, but the loss location can change for even smaller offsets. Therefore, SixTrack should be the tool of choice if an accurate tracking of light fragments is required.

We have shown that the STIER approach gives a good agreement with the measured loss pattern in the LHC. Nevertheless, the model could still be improved. Most notably, an online ion-matter interaction in all subsequent collimators could be included, as done for the LHC proton simulations carried out with SixTrack [8] or the SixTrack-FLUKA coupling [38]. This work is currently ongoing. Other possible improvements to the models include dedicated estimates of impact distributions on collimators for heavy-ion beams and studies of the influence of random machine imperfections.

The STIER simulations were benchmarked against the measured loss maps from the 3.5 Z TeV heavy-ion run. With upcoming operation with larger stored beam energies at 6.5 Z TeV and higher magnet currents, which imply a lower quench limit, the cleaning performance of the collimation system with heavy ions will become more critical. In these scenarios, it is crucial to have a well-benchmarked simulation tool that can be used to understand the performance limitations and overcome them. We have shown that STIER can serve this purpose, in spite of the inherent approximations.

STIER was used to validate the setting choices for the 2015 run with $^{208}Pb^{82+}$ ions, demonstrating that they were adequate. The analysis of the cleaning performance is still ongoing. On the longer term, the LHC will be upgraded to HL-LHC [39], which implies a further increase in the stored ion beam energy. STIER has been used to study these scenarios, in which it is believed that the machine performance will be limited by the heavy-ion collimation inefficiency. In this situation, the STIER simulations [33] demonstrate that the losses in the dispersion suppressor can be reduced to acceptable levels through the installation of extra collimators after the first dipoles, when the dispersion starts to rise [40–43].

Acknowledgements

We want to express our gratitude for valuable input and useful discussions to the FLUKA team, in particular F. Cerutti, A. Ferrari, A. Lechner and V. Vlachoudis. Work supported by the Wolfgang Gentner Programme of the BMBF.

References

[1] N. Holden, Development of the ICOSIM Program and Application to Magnetised Collimators in the LHC, Technical Report CERN-AB-Note-2008-054, CERN, Geneva, December 2008.
[2] H.H. Braun, et al., Collimation of heavy ion beams in LHC, in: Proceedings of EPAC 2004, Lucerne, Switzerland, (MOPLT010), 2004, p. 551.
[3] O. Brüning, et al., LHC Design Report (Volume I, The LHC Main Ring), CERN, 2004.
[4] W. Fischer, J.M. Jowett, Rev. Accel. Sci. Technol. 07 (2014) 49.
[5] B. Auchmann, et al., Phys. Rev. Accel. Beams 18 (0610002) (2015).
[6] R.W. Assmann, et al., The final collimation system for the LHC, in: Proceedings of EPAC 2006, Edinburgh, Scotland, (TUODFI01), 2006, pp. 986–988.
[7] R.W. Assmann, LHC Project Workshop – Chamonix XIV, 2005, p. 261.
[8] R. Bruce, et al., Simulations and measurements of beam loss patterns at the CERN Large Hadron Collider, Phys. Rev. ST Accel. Beams 17, 081004 (2014) 1-16.
[9] J.M. Jowett, et al., Proton-nucleus collisions in the LHC, in: Proceedings of IPAC 2013, Shanghai, China, (MOODB201), 2013, p. 49.
[10] J.M. Jowett, M. Schaumann, R. Versteegen, Future heavy-ion performance of the LHC, in: Review of LHC and Injector Upgrade Plans Workshop, 2013.
[11] J.M. Jowett, et al., First run of the LHC as a heavy-ion collider, in: Proceedings of IPAC 2011, San Sebastián, Spain, (TUPZ016), 2011, p. 1837.
[12] J.M. Jowett, et al., Heavy ions in 2012 and the programme up to 2022, in: Chamonix 2012 Workshop on LHC Performance, 2012.
[13] ATLAS Collaboration, J. Instrum. 3 (08) (2008) S08003.
[14] ALICE Collaboration, J. Instrum. 3 (08) (2008) S08002.
[15] CMS Collaboration, J. Instrum. 3 (08) (2008) S08004.
[16] LHCb Collaboration, J. Instrum. 3 (08) (2008) S08005.
[17] R. Bruce, R.W. Assmann, S. Redaelli, Phys. Rev. Accel. Beams 18 (June) (2015) 061001.
[18] R. Bruce, et al., Nucl. Instrum. Methods Phys. Res. Sect. A 729 (2013) 825.
[19] R.W. Assmann, et al., Summary of MD on Nominal Collimator Settings, CERN-ATS-Note-2011-036 MD, 2011.
[20] B. Salvachua, et al., LHC collimation cleaning and operation outlook, in: Proceedings of the 2012 Evian Workshop on LHC Beam Operation, CERN-ATS-2013-045, 2013.
[21] H.H. Braun, A. Fassò, A. Ferrari, J.M. Jowett, P.R. Sala, G.I. Smirnov, Phys. Rev. Accel. Beams 17 (February) (2014) 021006.
[22] S. Eidelman, et al., Phys. Lett. 1 (2004) B592.
[23] E.B. Holzer, et al., Development, production and testing of 4500 beam loss monitors, in: Proceedings of EPAC 2008, Genoa, Italy, (TUPC037), 2008, p. 1134.
[24] E.B. Holzer, et al., Beam loss monitoring system for the LHC, in: 2005 IEEE Nuclear Science Symposium Conference Record, vol. 2, 2005, pp. 1052–1056.
[25] W. Höfle, et al., Controlled transverse blow-up of high-energy proton beams for aperture measurements and loss maps, in: Proceedings of IPAC 2012, New Orleans, Louisiana, USA, (THPPR039), 2012, p. 4059.
[26] M. Sapinski, et al., Generation of controlled losses in millisecond timescale with transverse damper in LHC, in: Proceedings of IPAC 2013, Shanghai, China, (WEPME044), 2013, p. 3025.
[27] W. Höfle, et al., Transverse feedback: high intensity operation, AGC, IGC, Lessons for 2012, in: 3rd Evian Workshop on LHC beam operation, Evian-les-bains, France, 2011, pp. 97–100.
[28] R. Bruce, R.W. Assmann, G. Bellodi, C. Bracco, H.H. Braun, S. Gilardoni, E.B. Holzer, J.M. Jowett, S. Redaelli, T. Weiler, Phys. Rev. Accel. Beams 12 (January) (2009) 011001.
[29] T.T. Böhlen, F. Cerutti, M.P.W. Chin, A. Fassò, A. Ferrari, P.G. Ortega, A. Mairani, P.R. Sala, G. Smirnov, V. Vlachoudis, Nucl. Data Sheets 120 (2014) 211.
[30] A. Ferrari, P.R. Sala, A. Fasso, J. Ranft, FLUKA: A Multi-particle Transport Code (Program Version 2005), CERN-2005-10 (2005), INFN/TC_05/11, SLAC-R-773, 2005.
[31] MAD – Methodical Accelerator Design, ⟨http://cern.ch/madx/ (accessed 05.02.16).
[32] P.D. Hermes, et al., Studies on heavy ion losses from collimation cleaning at the LHC, in: Proceedings of HB 2014, East-Lansing, MI, USA, (MOPAB43), 2014, pp. 138–142.
[33] P.D. Hermes, R. Bruce, J.M. Jowett, S. Redaelli, Betatron cleaning for heavy ion beams with IR7 dispersion suppressor collimators, in: Proceedings of IPAC 2015, Richmond, VA, USA, (TUPTY025), 2015, pp. 2057–2059.
[34] F. Schmidt, SixTrack Version 4.2.16 Single Particle Tracking Code Treating Transverse Motion with Synchrotron Oscillations in a Symplectic Manner – User's Reference Manual, CERN/SL/94-56 (AP), 1994.
[35] G. Robert-Demolaize, et al., A new version of SixTrack with collimation and aperture interface, in: Proceedings of PAC 2005, Knoxville, Tennessee, USA, (FPAT081), 2005, p. 4084.
[36] T. Trenkler, J.B. Jeanneret, K2: A Software Package Evaluating Collimation Systems in Circular Colliders (Manual), CERN SL Note, SL/Note 94-105 (AP), 1994.
[37] C. Tambasco, An improved scattering routine for collimation tracking studies at LHC (Master's thesis), Universitá di Roma, CERN-THESIS-2014-014, 2014.
[38] A. Mereghetti, et al., SixTrack-FLUKA active coupling for the upgrade of the SPS scrapers, in: Proceedings of IPAC 2013, Shanghai, China, (WEPEA064), 2013, pp. 2657–2659.
[39] L. Rossi, LHC upgrade plans: options and strategy, in: Proceedings of IPAC 2011, San Sebastián, Spain, (TUYA02), 2011, pp. 908–912.
[40] R. Bruce, D. Bocian, S. Gilardoni, J.M. Jowett, Phys. Rev. Accel. Beams 12 (071002) (2009).
[41] T. Weiler, et al., Beam cleaning and beam loss control, in: Proceedings of HB 2008, Nashville, Tennessee, USA, (WGD08), 2008, pp. 359–362.
[42] R. Bruce, A. Marsili, S. Redaelli, Cleaning performance with 11 T dipoles and local dispersion suppressor collimation at the LHC, in: Proceedings of IPAC 2014, Dresden, Germany, (MOPRO042), 2014, pp. 170–173.
[43] A. Lechner, et al., Power deposition in LHC magnets with and without dispersion suppressor collimators downstream of the betatron cleaning insertion, in: Proceedings of IPAC 2014, Dresden, Germany, (MOPRO021), 2014, pp. 112–115.